

Anomalous nanoscale diffusion in Pt/Ti: superdiffusive intermixing

P. Süle, M. Menyhárd

Research Institute for Technical Physics and Material Science,
www.mfa.kfki.hu/~sule, sule@mfa.kfki.hu
Konkoly Thege u. 29-33, Budapest, Hungary

(Dated: 2007.10.24)

Probing the anomalous nanoscale intermixing using molecular dynamics (MD) simulations in Pt/Ti bilayer we characterize the superdiffusive nature of interfacial atomic transport. In particular, the low-energy (0.5 keV) ion-sputtering induced transient enhanced intermixing has been studied by MD simulations. *Ab initio* density functional calculations have been used to check and reparametrize the employed heteronuclear interatomic potential. We find a robust intermixing in Pt/Ti driven by nanoscale mass-anisotropy. The sum of the square of atomic displacements $\langle R^2 \rangle$ asymptotically scales nonlinearly ($\langle R^2 \rangle \propto t^2$), where t is the time of ion-sputtering, respectively which is the fingerprint of superdiffusive features. This anomalous behavior explains the high diffusivity tail in the concentration profile obtained by Auger electron spectroscopy depth profiling (AES-DP) analysis in Pt/Ti bilayer (reported in ref.: P. Süle, *et al.*, J. Appl. Phys., **101**, 043502 (2007)). In Ti/Pt bilayer a linear time scaling of $\langle R^2 \rangle \propto t$ has been found at the Ti/Pt interface indicating the suppression of superdiffusive features. These findings are inconsistent with the standard ion-mixing models. Instead a simple accelerative effect of the downward fluxes of energetic particles on the unidirectional fluxes of preferential intermixing of Pt atoms seems to explain the enhancement of interfacial broadening in Pt/Ti. Contrary to this in Ti/Pt the fluxes of recoils are in counterflow with intermixing Pt atoms and hence slows down the nanoscale mass-effect driven ballistic preferential mobility of Pt atoms.

PACS numbers: 66.30.Jt, 61.80.Jh, 68.35.-p, 68.35.Fx, 66.30.-h, 68.55.-a

I. INTRODUCTION

The nanoscale production of nano-devices constitute a topic of high current interest due to numerous potential applications^{1,2}. The construction of sharp interfaces in the nanoscale, however, faces many difficulties which requires the fundamental understanding of nanoscale interfacial diffusion³.

There are a growing number of evidences emerged in the last few years that anomalous nanoscale broadening of interfaces or high diffusivity tail in the impurity concentration profile occur during ion-irradiation⁴⁻¹⁰, sputter deposition of solids¹¹ or during thin film reactions and reactive front propagation^{12,13}. The anomalous nanoscale bulk diffusional effects could be due to still not clearly established accelerative effects leading to anomalously fast and possibly athermal diffusion at interfaces or during impurity diffusion^{4-12,14-24}.

Anomalous atomic transport (AAT) in the bulk or on surfaces can be categorized into few groups of phenomena: (i) Post-irradiation induced enhancement of impurity^{4,5} or dopant diffusion^{7,18-24} and transient enhanced interfacial broadening^{6,8-10}. Computer simulations reveal AAT during low-energy cluster and single-atomic deposition³¹. (ii) The amplification of intermixing during thin film growth (sputter deposition)^{11,31} or forced alloying¹⁴. (iii) Anomalous growth rates and front or interface propagation^{12,13}. (iv) Superdiffusion, random walk, Levy flight²⁵⁻²⁹ or quantum tunneling diffusion^{3,32} on solid surfaces. (v) Ultrafast atomic mobility with the coherent or collective movement of an en-

semble of atoms (not cluster diffusion)^{31,33-35}.

The physics behind these processes is not clearly established yet hence theoretical works are needed to model AAT which could explain the relation between the diversity of such processes. This is because AAT could not simply be explained by the conventional theories of atom movements, such as vacancy, interstitial diffusion, simple atomic site exchanges or hopping mechanisms^{3,28}. In the present paper we show that a simple explanation, such as atomic mass anisotropy induced amplification of ion-intermixing explains the occurrence of AAT in the prototypical mass-anisotropic system of Pt/Ti.

Computer atomistic simulations also reveal the occurrence of the enhancement of atomic transport upon ion-bombardment of various solids beyond a level explained by radiation enhanced diffusion^{9,33,36}. The characterization and understanding of the nanoscale amplification or weakening of atomic transport in the bulk, at interfaces and on the surface could be an important ingredient of the efficient production of nanostructures^{12,37}. In particular, it has been shown that nanoscale mass anisotropy influences seriously the sharpness of anisotropic interfaces^{9,36} as well as surface morphology^{29,30} and adatom yield²⁹.

Under forced conditions (such as low-energy ion-sputtering or ion-beam deposition, ball milling) otherwise not easily observable anomalous atomic transport processes can be amplified and could be detected. Such conditions have widely been applied in the last decades to force e.g. intermixing or alloying between immiscible elements^{14,17,38-41}. The athermal broadening of the

interface in strongly intermixing ion-irradiated bilayers such as Ni/Al and Cr/Al have been found which are inconsistent with the standard ion beam mixing models, such as ballistic, thermal spike or radiation enhanced diffusion⁶. In these materials, such as Ni/Al or Co/Al, the exothermic solid state reaction can even lead to extremely fast burn rates^{12,42}. The anomalously strong asymmetric ion-beam mixing has been found recently in Cr/Si multilayer using focused ion beam¹⁰.

Moreover, transient enhanced diffusion (TED) and intermixing have also been reported in post-annealed dopant implanted semiconductors^{18,20–24}. TED occurs when the depth distribution of the dopant exceeds the ion range⁴. Using low-energy ion-sputtering^{38,45,46} and Auger electron depth profiling analysis⁴⁰ it has been concluded recently that transient enhanced intermixing could occur in the film/substrate bilayer Pt/Ti while no such behavior is seen in the Ti/Pt bilayer, hence the magnitude of intermixing might depend on the succession of the film and the substrate⁹.

Anomalously long interdiffusion depths have been found in various diffusion couples^{4,6,11,18,20–24}. Transient enhanced intermixing has been reported in nonstoichiometric AlAs/GaAs quantum well structures⁴³ or in AsSb/GaSb superlattices⁴⁴ and has been attributed to vacancy or self-interstitial supersaturation in annealed samples. It has also been reported that in few cases anomalous intermixing is neither driven by bulk diffusion parameters nor by thermodynamic forces (such as heats of alloying)¹¹ or nor by heats of mixing^{36,47}. It has also been found that during low-energy ion-bombardment of bilayers the intermixing length (and the mixing efficiency) scales nonlinearly with the mass anisotropy (mass ratio) leading to the abrupt increase of the mixing efficiency in mass-anisotropic bilayers³⁶.

In the present work, computer atomistic simulations have been carried out to explain the occurrence of the ion-sputtering induced high diffusivity tail in the concentration profile of the film/substrate system of Pt/Ti. The enhanced intermixing in Pt/Ti reported in ref.⁹ is attempted to interpret as a superdiffusive atomic transport process since it fulfills the most important condition of superdiffusion: the square of atomic displacements scales nonlinearly with the time of IM²⁵. Superdiffusion has only been reported until now on solid surfaces^{26–28} and no reports have been found for bulk superdiffusion except for ultralight particles such as the migration of H in metals³.

We find the long range atomic transport of Pt in Ti is highly unusual and which could be explained as a mass anisotropy driven superdiffusive intermixing (SIM) process. Moreover, we conclude that SIM occurs due to the accelerative effect of unidirectional fluxes of energetic particles.

II. THE SETUP OF THE ATOMISTIC SIMULATIONS

Classical molecular dynamics simulations have been used to simulate the ion-solid interaction (using the PARCAS code⁵³). A variable timestep and the Berendsen temperature control is used to maintain the thermal equilibrium of the entire system.⁵⁴ The global coupling to the heat bath can be adjusted by the so called Berendsen temperature which we set to 70 K. Temperature control has been applied at the cell borders of the simulation cell to maintain constant temperature conditions. The bottom layers are held fixed in order to avoid the rotation of the cell. Since the z direction is open, rotation could start around the z axis. The bottom layer fixation is also required to prevent the translation of the cell. Periodic boundary conditions are imposed laterally and a free surface is left for the ion-impacts. The simulation uses the Gear's predictor-corrector algorithm to calculate atomic trajectories⁵⁴. The detailed description of other technical aspects of the MD simulations are given in refs.⁵³ and⁵⁴ and details specific to the current system in recent communications^{9,36,47}.

Our primary purpose is to simulate the conditions occur during ion-sputtering^{9,45} and Auger electron spectroscopy depth profiling analysis (AES-DP)⁹ using molecular dynamics simulations⁵⁴. Recently, MD simulation has been used to simulate ion-sputtering induced surface roughening^{30,48,49}. Following our previous work⁹ we ion bombard the bilayers Pt/Ti and Ti/Pt with 0.5 keV Ar⁺ ions repeatedly (consecutively) with a time interval of 10–20 ps between each of the ion-impacts at 300 K which we find sufficiently long time for most of the structural relaxations and the termination of atomic mixing, such as sputtering induced intermixing (IM)⁴⁷. Since we focus on the occurrence of transient intermixing atomic transport processes, the relaxation time of 10–20 ps should be appropriate for getting adequate information on transient enhanced intermixing. Pair potentials have been used for the interaction of the Ar⁺ ions with the metal atoms derived using *ab initio* density functional calculations.

The initial velocity direction of the impacting ion was 10 degrees with respect to the surface of the crystal (grazing angle of incidence) to avoid channeling directions and to simulate the conditions applied during ion-sputtering⁹. The impact positions have been randomly varied on the surface of the film/substrate system and the azimuth angle ϕ (the direction of the ion-beam). In order to simulate ion-sputtering a large number of ion irradiation are employed using script governed simulations conducted subsequently together with analyzing the history files (movie files) in each irradiation steps. In this article results are shown up to 150 ion irradiation (in a similar way to that given in ref.⁹). The impact positions of the 100–150 ions are randomly distributed over a $20 \times 20 \text{ \AA}^2$ area on the surface.

The volume of the cubic simulation cell is $110 \times 110 \times 90$

TABLE I: The parameters used in the tight binding potential given in Eqs. (1)-(2)⁵⁸

	ξ	q	A	p	r_0
Ti	1.416	1.643	0.074	11.418	2.95
Pt	2.695	4.004	0.298	10.612	2.78
Ti-Pt	4.2	2.822	0.149	11.015	2.87

^aThe parameters of the crosspotential have been obtained as follows⁵⁷: For the preexponentials ξ and A we used the harmonic mean $A_{TiPt} = (A_{Ti} \times A_{Pt})^{1/2}$ (ξ has been fitted to the *ab initio* curve shown in Fig. 1), for q and p we use the geometrical averages: $q_{TiPt} = (q_{Ti} + q_{Pt})/2$. The first neighbor distance of the Ti-Pt potential is given also as a geometrical mean of $r_0 = (r_0^{Pt} + r_0^{Ti})/2$.

\AA^3 including ~ 57000 atoms (with 9 monolayers (ML) film/substrate). The film and the substrate are ~ 20 and ~ 68 \AA thick, respectively. The setup of the simulation cell, in particular the 20 \AA film thickness is assumed to be appropriate for simulating broadening. Our experience shows that the variation of the film thickness does not affect the final result significantly, except if ultrathin film is used (e.g. if less than ~ 10 \AA thick film). At around 5 or less ML thick film surface roughening could affect mixing³⁰.

The (111) interface of the fcc crystal is parallel to (0001) of the hcp crystal and the close packed directions are parallel. The interfacial system has been created as follows: the hcp Ti is put by hand on the (111) Pt bulk (and vice versa) and various structures with different lateral sizes have been probed and are put together with fixed orientation mentioned above. This must be done to avoid built in stress in the initial structure. Therefore we put together slabs of the film and the substrate with different width while keeping (111) interfacial orientation. This is because the lattice mismatch is sensitive to the relative positions of the atoms at the interface. In order to minimize lattice misfit in the initial structure the relative lateral positions of the film and the substrate has been varied and the interfacial system with the smallest misfit strain has been selected. In fact this has been monitored via the starting average temperature of the system which indicates us how the generated structure is relaxed. The closer this temperature to 0 K the more relaxed the system is. The remaining misfit is properly minimized below $\sim 6\%$ during the relaxation process so that the Ti and Pt layers keep their original crystal structure and we get an atomically sharp interface. During the relaxation (equilibration) process the temperature is softly scaled down to zero and a sufficiently relaxed structure has been obtained. According to our practice we find that during the temperature scaling down the structure becomes sufficiently relaxed. Then the careful heating up of the system to 300 K has also been carried out. We believe that the lattice mismatch is minimized to the lowest possible level and we are convinced that no serious built-in stress remained in the simulation cell which could cause the explored anomalous atomic transport behaviors.

We used a tight-binding many body potential on the

basis of the second moment approximation (TB-SMA) to the density of states⁵⁸, to describe interatomic interactions. Within the TB-SMA, the band energy the attractive part of the potential reads,

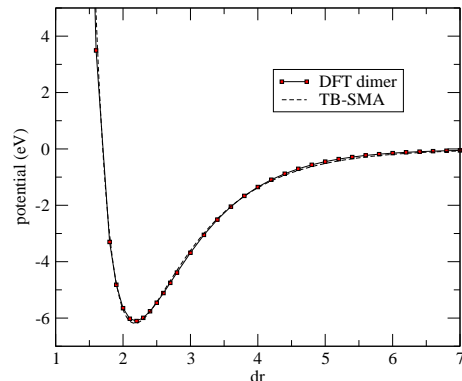


FIG. 1: The crosspotential energy (eV) for the Ti-Pt dimer as a function of the interatomic distance (\AA) obtained by the first-principles PBE/DFT method. For comparison the fitted interpolated TB-SMA potential is also shown calculated for the Ti-Pt dimer.

$$E_b^i = - \left[\sum_{j, r_{ij} < r_c} \xi^2 \exp \left[-2q \left(\frac{r_{ij}}{r_0} - 1 \right) \right] \right]^{1/2}, \quad (1)$$

where r_c is the cutoff radius of the interaction and r_0 is the first neighbor distance (atomic size parameter). The repulsive term is a Born-Mayer type phenomenological core-repulsion term:

$$E_r^i = A \sum_{j, r_{ij} < r_c} \exp \left[-p \left(\frac{r_{ij}}{r_0} - 1 \right) \right]. \quad (2)$$

The parameters (ξ, q, A, p, r_0) are fitted to experimental values of the cohesive energy, the lattice parameter, the bulk modulus and the elastic constants c_{11} , c_{12} and c_{44} ⁵⁸ and which are given in Table 1. r_{ij} is the internuclear separation between atoms i and j . The total cohesive energy of the system is

$$E_c = \sum_i^{Nat} (E_r^i + E_b^i), \quad (3)$$

where Nat is the number of atoms in the system.

The TB-SMA potential gives a good description of lattice vacancies, including atomic migration properties and a reasonable description of solid surfaces and melting⁵⁸. In ref.⁹ it has been shown that the TB-SMA potential gives the reasonable description of IM in Pt/Ti and gives interfacial broadening comparable with AES-DP measurements. Cutoff is imposed out of the 2nd nearest neighbors when the interatomic interactions have been

calculated which we find sufficient for simulating ion-mixing^{36,47}. Simulations have also been conducted using larger cutoff distances (up to 4th neighbors), however, no serious change has been observed in the final results.

An interpolation scheme has been employed for the crosspotential Ti-Pt^{9,29,36,57}. The employed potentials and the interpolation scheme for heteronuclear interactions have successfully been used for MD simulations^{36,50,55,56}. The Ti-Pt interatomic crosspotential of the TB-SMA potentials⁵⁸ type has been fitted recently to the experimental heat of mixing of the corresponding alloy system^{30,47}. The scaling factor r_0 (the heteronuclear first neighbor distance) is given as the average of the elemental first neighbor distances.

In this paper we use instead of our recent fit of the Ti-Pt potential⁴⁷ a more sophisticated potential. The crosspotential energy has been calculated for the Ti-Pt dimer using *ab initio* local spin density functional calculations⁵⁹ together with quadratic convergence self-consistent field (SCF) method. The G03 code is well suited for molecular calculations, hence it can be used for checking pair-potentials. The interatomic potential $V(dr)$ between two atoms is defined as the difference of total energy at an interatomic separation dr and the total energy of the isolated atoms

$$V(dr) = E(dr) - E(\infty). \quad (4)$$

The Kohn-Sham equations (based on density functional theory, DFT)⁶⁰ are solved in an atom centered Gaussian basis set and the core electrons are described by effective core potentials (using the LANL2DZ basis set)⁶¹ and we used the Perdew-Burke-Ernzerhof (PBE) gradient corrected exchange-correlation potential⁶². First principles calculations based on density functional theory (DFT) have been applied in various fields in the last few years⁶³.

The obtained profile is plotted in Fig. 1 together with our interpolated TB-SMA potential for the Ti-Pt dimer. We find that our interpolated TB-SMA potential nearly perfectly matches the *ab initio* one hence we are convinced that the TB-SMA model accurately describes the heteronuclear interaction in the Ti-Pt dimer. In fact we fitted only parameter $\xi = 4.2$, which influences the deepness of the potential well. The rest of the parameters are obtained using the interpolation scheme outlined in the caption of Table 1. We assume that this dimer potential is transferable for those cases when the Pt atom is embedded in Ti. This can be done because, as we outlined above, the interpolated Ti-Pt potential properly reproduces the available experimental results for the Ti-Pt alloy⁴⁷.

The crosssectional computer animations of simulated ion-sputtering can be seen in our web page⁶⁴. Further details are given in refs.^{9,36,47}.

III. RESULTS

The cartoons of the simulation cells (crosssectional slabs as a 3D view) can be seen in Fig. 2 which show the strong mixing at the interface in Fig. 1a (Pt/Ti) and a much weaker mixing in Fig. 1b (Ti/Pt).

In Fig. 3 the evolution of the sum of the square of atomic displacements (SD)

$$\langle R^2 \rangle = \sum_i^{N_{atom}} [\mathbf{r}_i(t) - \mathbf{r}_i(t=0)]^2, \quad (5)$$

of all intermixing atoms obtained by molecular dynamics simulations, where $(\mathbf{r}_i(t))$ is the position vector of atom 'i' at time t , N_{atom} is the total number of atoms included in the sum), can be followed as a function of the ion fluence. Lateral components (x, y) are excluded from

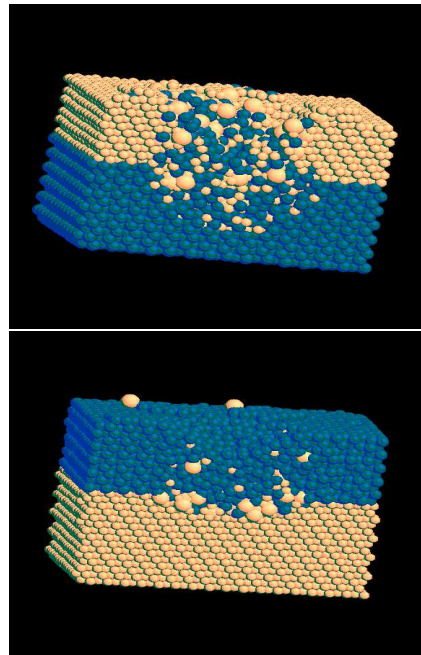


FIG. 2: The cartoons of the simulation cells after 100 ions bombardment as a crosssectional view (cut in the middle of the cell). The incorporated Ar^+ ions are also shown as larger light spheres. The smaller light and dark spheres denote the Pt and Ti atoms, respectively. Fig 2a: Pt/Ti, Fig 2b: Ti/Pt

$\langle R^2 \rangle$ and only contributions from IM atomic displacements perpendicular to the layers are included (z components). We follow during simulations the time evolution of $\langle R^2 \rangle$ which reflects the atomic migration through the interface (no other atomic transport processes are included). Note, that we do not calculate the mean square of atomic displacements (MSD) which is an averaged SD over the number of atoms included in the sum ($\text{MSD} = \langle R^2 \rangle / N_{atom}$). MSD does not reflect the real physics when localized events take place, e.g. when only few dozens of atoms are displaced and intermixed. In

such cases the division by N_{atom} , when N_{atom} is the total number of the atoms in the simulation cell leads to the meaningless $\langle R^2 \rangle / N_{atom} \rightarrow 0$ result when $N_{atom} \rightarrow \infty$, e.g. with the increasing number of atoms in the simulation cell. Also, it is hard to give the number of "active" particles which really take place in the transient atomic transport processes. Hence we prefer to use the more appropriate quantity SD. In Fig. 3 we present $\langle R^2 \rangle$ as a function of the number of ion impacts N_i (ion-number fluence). $\langle R^2 \rangle(N_i)$ corresponds to the final value of $\langle R^2 \rangle$ obtained during the N_i th simulation. The final relaxed structure of the simulation of the $(N_i - 1)$ th ion-bombardment is used as the input structure for the N_i th ion-irradiation. The asymmetry of mixing can clearly be seen when $\langle R^2 \rangle(N_i)$ and the depth profiles given in ref.⁹ are compared in Ti/Pt and in Pt/Ti. The computer an-

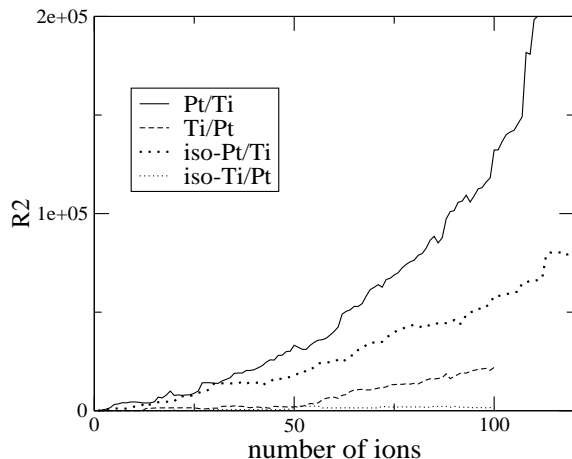


FIG. 3: The simulated square of IM atomic displacements $\langle R^2 \rangle$ (\AA^2) in Pt/Ti, Ti/Pt and in Cu/Co as a function of the ion-fluence (number of ions) obtained during the ion-sputtering of these bilayers at 500 eV ion energy (results are shown up to 100 ions). The dotted lines (iso-Pt/Ti and iso-Ti/Pt) denote the results obtained for the artificial mass-isotropic Pt/Ti and Ti/Pt bilayers, respectively.

imations of the simulations⁶⁴ together with the plotted broadening values at the interface in ref.⁹ also reveal the stronger IM in Pt/Ti. Moreover we find the strong divergence of $\langle R^2 \rangle$ from linear scaling for Pt/Ti while linear scaling has been found for Ti/Pt.

As it has already been shown in ref.⁹ AES-DP found a relatively weak IM in Ti/Pt (the interface broadening $\sigma \approx 20$ \AA) while an unusually high IM occurs in the Pt/Ti bilayer ($\sigma \approx 70$ \AA). MD simulations provide ~ 20 \AA and ~ 40 \AA thick interface after 200 ion impacts, respectively.

A. The effect of mass anisotropy

In order to clarify the mechanism of intermixing and to understand how much the interfacial anisotropy influ-

ences IM, simulations have been carried out with atomic mass ratio $\delta = m_{Pt}/m_{Ti}$, where m_{Pt} and m_{Ti} are the atomic masses, is artificially set to $\delta \approx 1$ (mass-isotropic). We find that $\langle R^2 \rangle$ is below the corresponding curve of Pt/Ti (see Fig. 3, iso-Pt/Ti, dotted line, see also the corresponding animation⁶⁴). The $\langle R^2 \rangle$ scales nearly linearly as a function of the number of ions (and with t) for iso-Pt/Ti. Hence the asymptotics of $\langle R^2 \rangle$ is sensitive to the effect of δ . We reach the conclusion that the mass-effect is robust and the magnitude of IM is weakened significantly. Actually the system undergoes the transition in the asymptotics of $\langle R^2 \rangle \propto t^2 \rightarrow \langle R^2 \rangle \propto t$. This finding together with our AES measurements (with the long-range tail shown in ref.⁹) confirms our recent results reported for various bilayers in which a strong correlation has been obtained between the experimental and simulated mixing efficiencies and mass anisotropy in various metallic bilayers³⁶. In that article we found that below a certain threshold mass ratio value ($\delta \leq 0.33$) the rate of intermixing increases abruptly³⁶. On the basis of the results obtained in this paper this surprising interdiffusive behavior of bilayers could be explained by the anomalous nature of mixing which can be tuned by the mass-anisotropy (mass ratio) of the systems. The experimentally observed mixing asymmetry can also partly be explained by the mass effect.

The interchange of atomic masses: To further test mass-effect on IM, we carried out simulations for the Pt/Ti system in which the atomic masses have been interchanged (Ti possesses the atomic mass of Pt and vice versa) setting in an artificial mass ratio (the inverse of the normal one). We find that this artificial setup of atomic masses results in the suppression of IM in Pt/Ti. Moreover, if we interchange the masses in Ti/Pt, we find strong IM and nonlinear scaling of $\langle R^2 \rangle$, while we find a much weaker one with natural atomic masses. The effect of mass anisotropy seems to be decisive in the occurrence of transient enhanced IM in Pt/Ti and of the asymmetry of IM.

IV. DISCUSSION

A. The nonlinear scaling of $\langle R^2 \rangle$

In recent papers we explained single-ion impact induced intermixing governed by the mass-anisotropy parameter (mass ratio) in these bilayers^{29,36}. It has already been shown in refs.^{36,47} that the backscattering of the light hyperthermal particles (BHP) at the mass-anisotropic interface leads to the increase in the energy density of the displacement cascade. We have found that the jumping rate of atoms through the interface is seriously affected by the mass-anisotropy of the interface when energetic atoms (hyperthermal particles) are present and which leads to the preferential IM of Pt to Ti^{36,47}.

Although we find in accordance with ref.³⁶ that ther-

mal spike occurs in both systems with the lifetime of few ps, however, we rule out thermal spike effects on IM in Pt/Ti. In particular, the observed insensitivity of IM to the choice of the heat of mixing ΔH in Ti/Pt⁴⁷ is in contrast with the thermal spike model³⁶. The appearance of $\langle R^2 \rangle \propto t^2$ scaling requires the presence of hyperthermal particles which are present only during the collisional cascade. These particles are also present in Ti/Pt, however in Pt/Ti we find the further acceleration of the hot atoms due to unknown origin.

We reach the conclusion that there must be an accelerative force field which speeds up few of the Pt particles to ballistic transport. The process must be active during the cascade. This is reflected by the divergence of $\langle R^2 \rangle$ from linear scaling in Fig. 3 for Pt/Ti. Interdiffusion

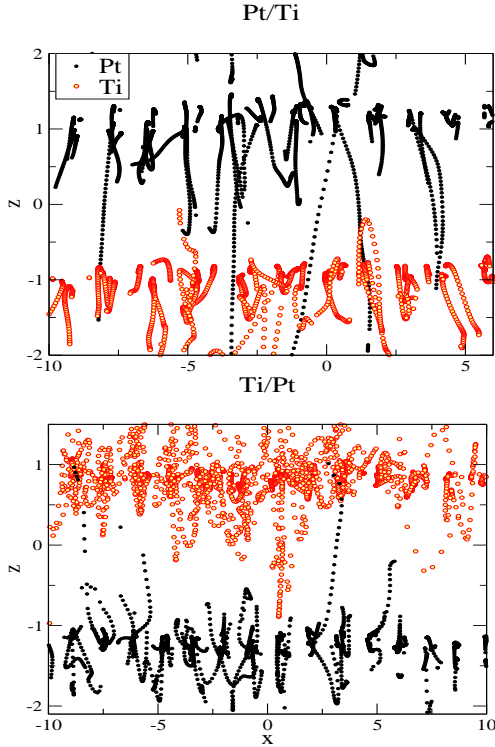


FIG. 4: The cross-sectional view of a typical collisional displacement cascade at the interface with atomic trajectories (two monolayers are shown at the interfaces as a cross-sectional slab cut in the middle of the simulation cell) in Pt/Ti (upper panel) and in Ti/Pt (lower panel). The positions of the energetic particles are collected up to 500 fs during a 500 eV single ion-impact event. The vertical axis corresponds to the depth position given in Å. The position $z = 0$ is the depth position of the interface. x is the horizontal position (Å).

takes place via ballistic jumps (ballistic mixing), when $\langle R^2 \rangle$ grows asymptotically as N^2 , where N is the number fluence (the same asymptotics holds as a function of ion-dose or ion-fluence). This can clearly be seen in Fig. 3 for Pt/Ti. The horizontal axis is proportional to the time of ion-sputtering, hence $\langle R^2 \rangle \propto t^2$ which is the time scaling of ballistic atomic transport²⁵.

In our particular case we follow the time evolution of the simulation cell after each of the ion impacts until $t \sim 10 - 20$ ps which we find sufficient time for the evolution of $\langle R^2 \rangle$. Anyhow, above this t value the asymptotics of $\langle R^2 \rangle(t)$ is invariant to the choice of the elapsed time/ion-bombardment induced evolution of $\langle R^2 \rangle(t)$. Hence the transformation between ion-fluence and time scale is allowed. $\langle R^2 \rangle \propto t^2$ and $\langle R^2 \rangle \propto t$ time scalings have been found even for the single-ion impacts averaged for few events (when $\langle R^2 \rangle(t)$ is plotted only for a single-ion impact) for Pt/Ti and Ti/Pt, respectively. The $\langle R^2 \rangle \propto t^n$, scaling, where $n \geq 2$, used to be considered as the signature of anomalous diffusion (superdiffusion) in the literature²⁵. Such kind of time scaling has been reported until now during the random walk or flight of particles and clusters on solid surfaces²⁵⁻²⁹. These processes are inherently athermal due to the vanishingly small activation energy of surface diffusion. We would like to show that it might also be the case that transient IM takes place in Pt/Ti which resembles in many respect the superdiffusive atomic transport processes known on solid surfaces²⁵.

In ref.⁹ the concentration profiles measured by Auger electron spectroscopy (AES) depth profiling analysis have been reported. The obtained results are in agreement with the findings presented in this article. However, in that paper it has not been realized that the fingerprint of superdiffusive feature of IM is detected by AES as a diffusivity tail in the concentration profile of Pt at the Pt/Ti interface in the Pt/Ti bilayer. No such tail occurs in the concentration profile of Ti/Pt shown in ref.⁹ where the profile can be characterized by "normal" *erf* functions. Hence we find that the succession of the film and substrate could determine the magnitude of IM (the asymmetry of IM).

No such ballistic behavior can be seen for Ti/Pt in Fig. 3. In Ti/Pt we find $\langle R^2 \rangle \propto t$ time scaling. The mean free path of the energetic particles are much shorter in Ti/Pt. This can be seen qualitatively in Fig. 4 if we compare the length of the atomic trajectories for Pt between upper and lower panels of Fig. 4. In the plot of Pt/Ti in Fig. 4 we can see ballistic trajectories which result in the superdiffusive spread of Pt atoms.

The trajectories of the reversed Ti recoils can be seen in upper Fig. 4 and no intermixing Ti atomic positions can be found in the upper panel of Fig. 4 (Ti/Pt). Although, Fig. 4 has no any statistical meaning, however, the atomic trajectories are plotted from a typical cascade event hence some useful information can be obtained for the transport properties of energetic Pt atoms. In the lower panel of Fig. 4 we can see the ballistic trajectories of intermixing hyperthermal Pt atoms (Pt/Ti). The reversed Ti particles at the interface and the weaker IM of Pt atoms to the Ti phase result in the weaker IM in Ti/Pt than in the Pt/Ti system. Hence Fig. 4 depicts us at atomistic level what we see in the more statistical quantity $\langle R^2 \rangle$. In Ti/Pt we see much shorter inter-layer atomic trajectories while in Pt/Ti ballistic trajectories of

Pt atoms can be seen (moving through the interface).

B. The ballistic model: deposited energy

The ballistic model and the ballistic regime in the collisional cascade can also be ruled out as the source of the asymmetry of IM. We calculated the magnitude of the total deposited energy F_D in Pt and in Ti, and get the values of 127.6 and 148.5 eV for Pt/Ti and for Ti/Pt, respectively at 0.5 keV incident ion energy. Although the F_D is larger in Ti/Pt, the intermixing is weaker in this material. Using TRIDYN calculations one can estimate the magnitude of the deposited energy at the interface^{38,51,52}. We calculate few eV/Å at the interface and again F_D is smaller in the case of Pt/Ti. We conclude from this that not the larger F_D and the smaller stopping power of Pt causes the anomalous IM in Pt/Ti.

The larger the E_d smaller the number of displaced atoms n_d at the interface which leads to smaller F_D following the Kinchin-Pease formula of $F_D = 2n_d E_d$ ³⁹. Although we have no values for n_d in various materials, however, the corresponding E_d values for Pt (33 eV) and Ti (19 eV) can be found in text books³⁸. One can see that the E_d of Pt is much larger than that of Ti, which again suggest that simply if we rely only on the ballistic model we expect larger IM in Ti/Pt. This is because such a big difference in E_d values would strongly suggest that much larger IM should occur in Ti/Pt than in Pt/Ti. Also we can expect that the number of Frenkel pairs is much larger in Ti than in Pt under the same irradiation conditions. The Kinchin-Pease formula should give somewhat larger F_D for Ti/Pt. However, we get comparable values as obtained by MD and SRIM simulations. Then we can conclude that the difference in the deposited energy at the interface can not be the reason of IM amplification in Pt/Ti.

Also, at low-energy ion bombardment of 500 eV the deposited energy at the depth of the interface (few eV) is insufficient to create Frenkel pairs (few tens of eV). Hence this energy is dissipated into the lattice which leads to local thermalization. On the other hand displaced atoms close to the surface of the film if becomes not sputtered atoms, travel towards the interface as recoils. These recoils create second or higher order generation of energetic atoms. However, at this low incident ion energy regime the mean free path of these atoms do not exceed the distance of few times of the lattice constant. Hence their direct effect at the interface is negligible and these ballistic collisions of the recoils with the lattice atoms can not cause TED in Pt/Ti. The simulated nonlinear time evolution of $\langle R^2 \rangle$ indicates the acceleration of particles. During the cascade intermixing of particles with the mass ratio of $\delta \approx 1$ no such nonlinear scaling of $\langle R^2 \rangle$ can be found. This is because particles with nearly equal masses loose their kinetic energy during elastic collisions and the lifetime of the cascade and spike period remains short and which does not allow the evolution of $\langle R^2 \rangle \propto t^2$ time scal-

ing. Hence from the conventional picture of collisional cascades no intermixing acceleration can be expected.

The projectile-to-target mass ratio could also play some role in the magnitude of F_D at the interface³⁸. Due to the large mass difference in the case of $Ar^+ \rightarrow$ Pt (Pt/Ti) elastic collisions the energy loss is larger than for $Ar^+ \rightarrow$ Ti impacts (Ti/Pt). Contrary to this we get the stronger IM in Pt/Ti. It seems again that not simple binary collision effects the reason of the asymmetry of IM.

C. Thermal spike: heat of mixing

In recent publications we have already shown that we find the lack of the effect of heat of mixing ΔH of the corresponding alloy phases on ion-mixing in Ti/Pt⁴⁷. This is in contrast with the predictions of the thermal spike model which suggest that ΔH governs intermixing during the ion bombardment of various bilayers^{38,39,65}. Repeating simulated ion-sputtering with varying ΔH in Pt/Ti, we find again that the magnitude of ion-mixing is insensitive to the choice of the ΔH which can be tuned by adjusting parameter ξ (the preexponential parameter in the attractive term in Eq. (1))⁴⁷. Even if $\Delta H \approx 0$ ($\xi = 0$) strong IM occurs, although in the alloy phase decomposition takes place. Therefore the influence of thermodynamic driving forces can be ruled out and we conclude that the thermal spike model might not be consistent with the occurrence of TED in Pt/Ti.

D. Radiation enhanced diffusion: TED is athermal

Since neither the ballistic nor the TS model are consistent with our findings in Pt/Ti we check whether other system parameters govern IM. First, we discuss, whether the thermally activated radiation enhanced diffusion, which usually takes place after the TS period is responsible for the asymmetry of IM in Pt/Ti and in Ti/Pt. No temperature dependence has been found. The simulations provide nearly the same results in ~ 0 K and at room temperature events. Large athermal experimental mixing rates ($k > 10^4 \text{ Å}^4$) have also been found for Ni/Al, Cu/Al and Al/Mo bilayers by other groups^{6,66,67}. These results are inconsistent with the operation of RED induced TED in these materials^{6,38}. Because of the insensitivity of TED in Pt/Ti to temperature effects we can also rule out the influence of any conventional thermally activated vacancy and interstitial diffusion mechanisms³.

E. The proposed mechanism

The radiation induced enhancement of IM in Ti/Pt has been studied in detail in ref.⁴⁷. The mass anisotropic interface stops the light energetic particles which leads to overheating in the Ti phase in Ti/Pt. This leads to the

temporal decoupling of the IM of Pt and Ti with the preferential IM of Pt⁴⁷. The IM of Ti is delayed to the end of the TS period (retarded IM)⁴⁷. In Ti/Pt the IM of Pt atoms take place, however, upwards to the film against the downward ion and recoil fluxes which slows down IM. In Pt/Ti, however, the preferential IM of Pt goes downwards to the substrate accelerated by the unidirectional incoming ions and displaced energetic atoms. Hence the heavier particle Pt behaves like a ballistic first diffuser in Pt/Ti and as a slowed down particle by the counterflow of downward moving (from the film towards the substrate) energetic particles of ion irradiation in Ti/Pt.

The ballistic preferential IM of Pt is governed by mass effect: the light energetic particles (Ti) are backscattered at the heavy interface leading to the retardation of IM of them⁴⁷. Also, the reversed flux of the light particles

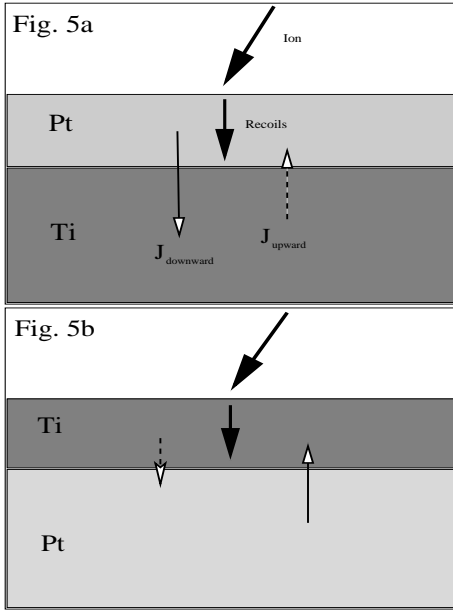


FIG. 5: The schematic diagram of various ion-sputtering induced fluxes occur in a general mass-anisotropic film/substrate bilayer. Intermixing fluxes at the interface correspond to $J_{\uparrow,S}(\delta)$ (with upward arrow) and $J_{\downarrow,F}(\delta)$ (downward arrow) while the downward arrow in the film to the recoil flux of J_{\downarrow}^{rec} . This configuration holds for $m_F \gg m_S$ where m_F and m_S denote the atomic masses of the film and substrate constituents, respectively (FIG. 5a corresponds to Pt/Ti). Note the unidirectional fluxes of J_{\downarrow}^{rec} and $J_{\downarrow,F}(\delta)$. Moreover, fluxes $J_{\uparrow,S}(\delta)$ and $J_{\downarrow,F}(\delta)$ are decoupled in time as it has been shown in ref.⁴⁷: the mass current of Pt atoms $J_{\downarrow,F}(\delta)$ goes predominantly while $J_{\uparrow,S}(\delta)$ is delayed by few ps. FIG. 5b (Ti/Pt): In this case fluxes J_{\downarrow}^{rec} and $J_{\uparrow,S}(\delta)$ (IM Pt atoms) are in opposite direction hence weakens each others effect which leads to the suppression of IM. This situation corresponds to the case when $m_F \ll m_S$.

increases the energy density in the Ti phase promoting the IM of the Pt atoms.

Therefore we find the ion irradiation induced athermal preferential intermixing of Pt atoms in Pt/Ti. Two

accelerating effects amplify each others effect: the mass effect induced preferential interfacial mixing of energetic Pt atoms and the downward fluxes of the incident ions and recoils contribute to ballistic IM in Pt/Ti and to the emergence of nonlinear time scaling of $\langle R^2 \rangle$. The mass anisotropy induced enhancement of preferential Pt interdiffusion occurs in both bilayers, however, in Ti/Pt the fluxes of IM ballistic Pt atoms are somewhat slowed down by the counterflow of the downward movement of recoils. These simple reasonings explain the emergence of the asymmetry of IM with respect to the interchange of film and substrate constituents.

F. Phenomenology for δ -driven TED

The phenomenological description of the asymmetric TED might help in understanding and explaining the results obtained by experiment and MD simulations. Following the Martin's theory of irradiation induced ballistic diffusion⁶⁸ and the Cahn-Hilliard theory of thermal diffusion⁶⁹ the diffusion constant can be written formally as the sum of thermally activated and ballistic (athermal) terms⁶⁸:

$$D_{irrad} = D_{th}(T) + D_{\downarrow}^{rec}. \quad (6)$$

The interdiffusion drift due to cascade mixing with recoils (hyperthermal particles) is given via D_{\downarrow}^{rec} . Within our picture of TED the mass effect induced amplification of IM over the thermal and cascade mixing rates can be written as

$$D_{TED}(T, \delta) = D_{th}(T) + D_{\downarrow}^{rec} + D_{enhan}(\delta), \quad (7)$$

where $D_{th}(T)$ is a normal thermally activated diffusion constant, where T is the temperature in the thermal spike (irradiation induced molten phase) and $D_{enhan}(\delta)$ is an enhancement term depending on δ . This model explains TED as an amplification of atomic intermixing on top of radiation enhanced diffusion (thermally activated and collisional cascade ballistic interdiffusion $D_{RED} = D_{th}(T) + D_{\downarrow}^{rec}$. Eq. 7 should give $D = D_{th} + D_{\downarrow}^{rec}$ when $\delta \approx 1$. It is not our intention in this paper to derive an explicit analytic expression which could reproduce the MD results (nonlinear time scaling of $\langle R^2 \rangle$ in Pt/Ti) as well as the experimental IM depth (long range diffusivity tail) in the concentration profile. Simply we would like to explain in detail the mechanism of TED within a phenomenological picture which helps understanding the amplification of IM.

Unidirectional and counterflow atomic flux: One possible way is to model mass effect by taking into account the counterflow ballistic intermixing mass flows J_{\uparrow} and J_{\downarrow} normal to the surface appear during ion-sputtering of bilayer systems. As mentioned above particle flow of heavy particles (Pt) takes place downwards in Pt/Ti and upwards in Ti/Pt. The total mass flow is the sum of these terms,

$$J(\delta) = J_{\uparrow,A}(\delta) + J_{\downarrow,B}(\delta) + J_{\downarrow}^{rec}, \quad (8)$$

where $J_{\uparrow,A}$ and $J_{\downarrow,B}$ are the intermixing mass flow of constituents A and B through the interface (the interface currents in a A/B bilayer, respectively). The term J_{\downarrow}^{rec} is the downward flux of energetic particles occurs upon external forced conditions (ion-sputtering) towards the interface. This term corresponds to the case when $\delta \approx 1$. The δ -induced downward flux amplification is $\Delta J(\delta) = J_{\downarrow,B}(\delta) - J_{\downarrow}^{rec}$, which leads to superdiffusion. The schematic view of the fluxes is shown in Fig. 5 for a situation, when the film component (F) is B and the substrate (S) is A. Heavy particles have the tendency to IM preferentially over the light components⁴⁷ which results in $J_{Pt} > J_{Ti}$. In Pt/Ti, $J_{\downarrow,B}(\delta) = J_{Pt}$, while in Ti/Pt $J_{\uparrow,A}(\delta) = J_{Pt}$. It has also been shown recently that the IM of the light and heavy components is decoupled in time by few ps due to the predominant IM of the heavy atoms⁴⁷ which results in the robust amplification of the interface current of Pt $J_{Pt} \gg J_{Ti}$.

Intermixing atomic fluxes $J_{\uparrow,A}$ and $J_{\downarrow,B}$ (see Fig. 5) are created indirectly upon ion-sputtering, while flux J_{\downarrow}^{rec} appears directly upon ion-bombardment. However, $J_{\uparrow,A}(\delta)$ and $J_{\downarrow,B}(\delta)$ are directly tuned by δ , while flux J_{\downarrow}^{rec} is nearly independent of δ . This is because flux J_{\downarrow}^{rec} appears in the film while the IM fluxes operate at the interface, where mass-anisotropy influences atomic transport directly. This rationalizes the separation of ion-induced atomic fluxes into δ -dependent and independent terms. If $\delta \rightarrow 1$, the sum of fluxes $J_{\uparrow,A} + J_{\downarrow,B} \approx 0$ vanishes and $J = J_{\downarrow}^{rec}$. The δ -independent part of Eq. 8 is simply the fluxes of cascade mixing term. Fluxes J_{\downarrow}^{rec} and $J_{\downarrow,B}(\delta)$ appear nearly in the same time (ballistic or cascade period), although flux $J_{\downarrow,B}(\delta)$ is induced by J_{\downarrow}^{rec} . This is because the mass-anisotropic system gives an ultrafast response to ion-irradiation and the $J_{\downarrow,Pt}(\delta)$ flux in Pt/Ti and $J_{\uparrow,Pt}(\delta)$ in Ti/Pt occur due to downwards recoils and flux J_{\downarrow}^{rec} .

δ -driven particle acceleration: J_{\downarrow}^{rec} and $J_{\downarrow,B}(\delta)$ are unidirectional in Pt/Ti, hence the ion-irradiation induced flux J_{\downarrow}^{rec} accelerates Pt atoms in Pt/Ti and slows down δ -driven IM in Ti/Pt because J_{\downarrow}^{rec} and $J_{\uparrow,A}$ are in contrary direction and nearly counteract or weakens each others effect. The impinging ions always generate energetic particles with downward momentum which is added to the momentum of δ -driven heavy particles leading to the huge amplification of atomic mobility of few intermixing atoms. Hence we explain the huge interfacial broadening in Pt/Ti by the cumulative effect of the two types of downward atomic mobilities.

The net intermixing mass flow can be described by the Fick's first law³,

$$\Delta J(\delta) = -\frac{\partial c}{\partial z}(D_{\uparrow}(\delta) - D_{\downarrow}(\delta)), \quad (9)$$

where the concentration gradient occurs due to the mass anisotropy⁴⁷. The thermal term does not lead to concentration difference and the broadening at the interface is symmetrical, the IM of the components is nearly the

same on both side of the interface. The athermal inter-diffusion drift is the balance of the upward and downward mass transport driven by δ and characterized by the ballistic diffusion constants $D_{\uparrow}(\delta)$ and $D_{\downarrow}(\delta)$.

Finally the amplification term of TED for the diffusion constant can be given as

$$D_{enhan}(\delta) = -(J_{\downarrow}(\delta) - J_{\downarrow}^{rec}) \left(\frac{\partial c}{\partial z} \right)^{-1}. \quad (10)$$

Therefore, if $\delta = 1$, purely thermally activated diffusion (atomic transport) takes place. If $\delta \gg 1$, TED occurs (the amplification factor $D_{enhan}(\delta) \gg D_{RED}$). When $\delta < 1$, TED features are suppressed, although we get a stronger IM than in the case of mass isotropy $\delta \approx 1$ ($D_{enhan}(\delta) \approx D_{RED}$).

G. Superdiffusion

Superdiffusive features, have never been reported before for intermixing, only for e.g. random walk of adatoms and clusters (Levy flight) on solid surfaces²⁵⁻²⁸. Transient mobility in the bulk has long been known only in collisional cascades^{38,39,45} during quantum diffusion of light particles³ or in shock loaded and stressed systems³. However, these bulk phenomena are driven mostly by external stimulus (cascades, thermal spike, shock loaded rearrangements) and can be characterized as driven systems^{14,68}. The only exception is the ultra low temperature ballistic diffusion of light particles in the lattice which is driven by (intrinsic) quantum effects³. Brockmann *et al.* has been attempted to interpret reacting particle systems with front propagation driven by reaction-superdiffusion¹³.

The mass anisotropy driven TED in Pt/Ti can also be considered as a driven system. In $\delta > 1$ systems the strong mass anisotropy driven acceleration of the particles leads to superdiffusion of the heavier atoms. However, the observed acceleration of the heavy particles is an intrinsic feature of $\delta > 1$ systems. The situation is somewhat similar to that found in the anomalous impurity diffusion of N in stainless steel⁴ and the observed large IM depths in various transition metal/Al diffusion couples¹¹ which could also be understood as super-interdiffusive processes. In Ni/Al bi-, multi-, and marker layers an unusually high mixing rate has been observed and which could not be understood within the picture of standard ion mixing models⁶ as well as in our case in Pt/Ti. These results suggest that anomalous and superdiffusive mass transport could occur in various driven systems in which still unknown intrinsic system parameters govern TED. These parameters exist independently from the externally forced condition (ion bombardment). The external perturbation of these systems is necessary, however, to induce the transient atomic rearrangements.

The superdiffusive features can be tuned by adjusting the mass ratio δ in Pt/Ti. Setting in artificial mass

isotropy, the nonlinear scaling of $\langle R^2 \rangle$ vanishes (see Fig. 3). Hence mass anisotropy δ operates as a system parameter ($\delta = m_{\text{film}}/m_{\text{substrate}}$, where the atomic mass of the film has been divided by the atomic mass of the substrate atoms), If $\delta \gg 1$, super-interdiffusion appears, however, if $\delta \leq 1$, IM slows down because of the counterflow of incident particles with IM Pt atoms. In ref.³⁶ it has been shown, that the mixing efficiency k/F_D , where k is the mixing rate ($k = \langle R^2 \rangle / \Phi$) and F_D and Φ are the deposited energy at the interface and the ion fluence, respectively³⁹, scales nonlinearly with δ . At $\delta < 0.33$ k/F_D increases abruptly. In that article we studied the ion mixing of A/B bilayers with $\delta \leq 1$. However, we did not study the inverted systems (B/A, $\delta > 1$, film atoms are much heavier than the substrate one). In B/A systems in general, in which $\delta \gg 1$, mass anisotropy driven superdiffusion might occur on the basis of the present results. This can be shown by computer experiments: if we simulate ion-mixing in mass isotropic systems, such as Co/Cu e.g., we get a very weak interfacial mixing. However, if we set in artificially $\delta \gg 1$, strong IM takes place as in Pt/Ti. We reach the conclusion that the simple system parameter δ governs the enhancement of IM in mass anisotropic bilayers. In the inverted case (A/B), when the lighter constituents are placed in the film, no transient enhanced intermixing occurs.

V. CONCLUSIONS

The most important findings are the following:

(i) *Mass effect and asymmetric mixing*: We find a robust mass effect on interfacial mixing in Pt/Ti which supports our finding published in ref.³⁶ in which a strong mass effect on ion-beam intermixing (IM) has been found for various mass-anisotropic bilayers. In order to increase the credibility of the employed computational approach, we fitted the crossinteraction atomic interaction potential to that of obtained from first principles calculations.

(ii) *Nonlinear time scaling*: We find that the sum of the squares of atomic displacements through the anisotropic interface ($\langle R^2 \rangle$) scales nonlinearly in Pt/Ti ($\langle R^2 \rangle \propto t^2$) as a function of the time (and the ion-number fluence) as shown in Fig. 3. The nonlinear time scaling of $\langle R^2 \rangle$ together with the long range (high diffusivity) tail in the AES profile shown in ref.⁹ might support the operation of a superdiffusive transport (athermal) process of Pt atoms in Pt/Ti. In Ti/Pt a nearly linear scaling ($\langle R^2 \rangle \propto t$) is found. The lack of a tail in the AES concentration profile for Ti/Pt⁽⁹⁾ is explained by the suppression of the preferential IM of Pt into the Ti phase due to the counterflow fluxes of downward moving recoils and the upwards mobility Pt atoms.

(iii) *Preferential mixing of Pt and further acceleration*: The atomistic mechanism of the asymmetry and TED in Pt/Ti is the following: The mass-anisotropy induced predominant intermixing of the heavier Pt atoms into the Ti phase has been found in both materials in accor-

dance with previous findings⁴⁷. The new finding is that in Ti/Pt the Pt atoms slow down during IM because of the slowing down effect of the counterflow of the incident energetic particles (recoils) during the cascade period. In Pt/Ti we find the contrary situation: the IM Pt atoms are accelerated by the unidirectional current of the hyperthermal particles (downward Pt recoils), hence the originally already preferentially intermixing Pt atoms even further accelerated. Hence the superdiffusion of these particles is driven by double acceleration: first driven by the mass ratio induced preferential transport and additionally by the ballistic particles in the collisional cascade with downward mobility (their momentum directed from the film towards the substrate). Such kind of an acceleration of particles in the bulk has never been reported before at best of our knowledge, although, this situation can be rather general in $\delta > 1$ systems.

The phenomenon is governed by the intrinsic system parameter mass anisotropy and not or only weakly influenced by external parameters, such as the ion specie, projectile to target mass ratio, the ion energy above few hundred eV or the external temperature. This is because the process requires only a unidirectional current of energetic particles with different origin, which is present in the system nearly independently from the parameters mentioned above. In this sense this unique feature of the superdiffusive TED makes it different from other ballistic atomic transport processes occurring in e.g. collisional cascades which strongly influenced by external parameters.

(iv) *Unconventional mechanism*: We conclude that the observed and simulated long range depth distribution of Pt atoms in the Ti phase of Pt/Ti cannot be understood by any established mechanisms of radiation-enhanced diffusion (RED). We find that the occurrence of the long range diffusivity tail, whose penetration depth exceeds the ion range could be understood as a superdiffusive process in the bulk. Moreover, normally, RED could not lead to the asymmetry of IM. That is because intermixing in the collisional cascade is normally insensitive to the succession of the layers. Also, the thermal spike (which is rather short at this ion energy) in principle could not provide asymmetric IM. Instead we speculate on the possible operation of accelerative effects which could enhance atomic mixing and penetration. The divergence of $\langle R^2 \rangle$ clearly indicates that accelerative effects are present in the lattice leading to ballistic transport. $\langle R^2 \rangle \propto t^2$ is the signature of ballistic atomic transport²⁵. The time evolution of nonlinear time scaling of $\langle R^2 \rangle$ requires the sufficiently large number of ballistic particles with large mean free path during most of the cascade events. During the "normal" cascade events of Ti/Pt $\langle R^2 \rangle$ does not exceed linear scaling. Hence a specific mechanism might come into play which speeds up Pt particles in the Ti bulk or at the interface during the collisional cascade period in Pt/Ti.

(v) *Unidirectional energetic atomic fluxes*: The δ -driven TED has also been explained using a phenomeno-

logical model based on a simple Fickian model. This helps in explaining the occurrence of the established accelerative effect on IM driven by unidirectional atomic fluxes. The fluxes of energetic particles can be separated into δ -dependent and independent terms. The corresponding diffusion constant is constructed as a sum of thermally activated, cascade (recoil) mixing and δ -dependent parts. The unidirectional fluxes in Pt/Ti leads to huge amplification of downwards fluxes while in Ti/Pt these fluxes are in counterflow direction leading to the weakening of the upwards intermixing fluxes of Pt atoms.

(vi) *The δ -driven AAT might be a general mechanism:* Finally we conclude that the established mechanism of TED might not be a specific one in nature. *Nanoscale mass-anisotropy* induced AAT could be a general feature of various multicomponent systems and could occur during the ion-beam processing (ion-sputtering, dopant implantation or ion-beam deposition) in various thin film multilayers, nanoinclusions, nanoislands, quantumdots embedded in light atomic host matrices (substrates) or in quantum well structures. Such kind of nanostructures and processing technologies are widely used in the production of heterostructure nanodevices¹ or magnetic nano-objects which are of high current interest due to numerous potential applications in various fields².

In particular, TED has been found in nonstoichiometric AlAs/GaAs quantum well structures⁴³ or in AsSb/GaSb superlattices⁴⁴ which can be considered as nanoscale mass-anisotropic systems with well-defined interfaces. The reported AAT in these systems could also be, at least partly, due to δ -driven AAT mechanism. Also, possibly there are couple of other systems in which the δ -driven AAT could take place. Just to mention few exam-

ples: sputter deposition of transition metals on Al^{11,31}, low energy cluster deposition and pinning on various substrates³¹. In these system it has already been shown by computer simulations that a δ -driven AAT mechanism plays a significant role during thin film growth³¹.

The most important structural condition which must be fullfield is that the occurrence of δ -driven TED requires the presence of a mass-anisotropic interface with $\delta \gg 1$. Hence when the primary goal is the production of nanostructured surfaces sharp interfaces are required for the efficient operation of nanodevices. According to our results, however, nanoscale mass-anisotropy might deteriorate the sharpness of mass-anisotropic interfaces, especially when ion-sputtering have been used during the processing of the nanostructured surfaces and interfaces. One possible way of avoiding δ -driven interface broadening is the construction of $\delta \leq 1$ multilayer thin films which do not allow the amplification of intermixing and even lead to the suppression of interdiffusion as it has been found in the Ti/Pt bilayer. The better understanding of δ -driven AAT could help in the more efficient production of nanothin films with sharp interfaces.

This work is supported by the OTKA grant F037710 from the Hungarian Academy of Sciences. We wish to thank to K. Nordlund for helpful discussions and constant help. The work has been performed partly under the project HPC-EUROPA (RII3-CT-2003-506079) with the support of the European Community using the supercomputing facility at CINECA in Bologna. The help of the NKFP project of 3A/071/2004 is also acknowledged. The G03 code is available at NIIF center at Budapest.

-
- ¹ V.A. Schukin, N. N. Ledentsov, D. Bimberg, *Epitaxy of Nanostructures*, Springer (2004).
 - ² K. Sumiyama, T. Hihara, D. L. Peng, and S. Yamamuro, *Encyclopedia of Nanoscience and Nanotechnology*, edited by H. S. Nalwa, Vol. 10, (2004).
 - ³ J. Philibert, *Atom Movements: Diffusion and Mass Transport in Solids*, (Les Edition de Physique, Les Ulis, France 1991), H. Mehrer, *Diffusion in Solids*, Fundamentals, Methods, Materials, Diffusion-Controlled Processes, Springer Series in Solid-State Sciences, Vol. 155 (2007).
 - ⁴ G. Abrasonis, W. Möller, X. X. Ma, Phys. Rev. Lett. **96**, 065901-1, (2006).
 - ⁵ S. Parascandola, W. Möller, D. L. Williamson, Appl. Phys. Lett., **76**, 2194 (2000), T. Telbizova, S. Parascandola, U. Kreissig, R. Günzel, and W. Möller Appl. Phys. Lett. **76**, 1404 (2000).
 - ⁶ N. Bibic, V. Milinovic, K. P. Lieb, M. Milosavljevic, and F. Schrempel, Appl. Phys. Lett. **90**, 051901 (2007), T. Weber, K.-P. Lieb, J. Appl. Phys., **73**, 3499 (1993), F. Shi, W. Bolse, K.-P. Lieb, J. Appl. Phys. **78**, 2303 (1995). H. K. Kim, S. O. Kim, J. H. Song, K. W. Kim, J. J. Woo, C. N. Whang and R. J. Smith, Nucl. Instr. and Meth. in Phys. Res. **B59-60**, 554. (1991).
 - ⁷ J. Cardenas, B. G. Svensson, W.-X. Ni, K. B. Joelson, G. V. Hansson, Appl. Phys. Lett., **73**, 3088 (1998).
 - ⁸ W. Nieven, B. W. Schueler, G. Goodman, P. Schnabel, J. Mosquito, I. Mowat, G. Chao, Appl. Surf. Sci., **231-232**, 13067 (1989).
 - ⁹ P. Süle, M. Menyhárd, L. Kótis, J. Lábár, J. F. Egelhoff Jr., J. Appl. Phys., **101**, 043502 (2007).
 - ¹⁰ Á. Barna, L. Kótis, J. Lábár, Z. Osváth, A. L. Tóth, M. Menyhárd, A. Zalar, P. Panjan, J. Appl. Phys., in press, **102**, (2007)
 - ¹¹ J. D. R. Buchanan, T. P. A. Hase, B. K. Tanner, P. J. Chen, L. Gan, C. J. Powell, and W. F. Egelhoff, Jr. Phys. Rev. **B66**, 104427 (2002).
 - ¹² V. Vovk, G. Schmitz, R. Kirchheim, Phys. Rev. **B69**, 104102 (2004).
 - ¹³ D. Brockmann, L. Hufnagel, Phys. Rev. Lett., **98**, 178301-1 (2007).
 - ¹⁴ P. Bellon, R. S. Averback, S. Odunuga, Y. Li, and P. Krasnochtchekov, Phys. Rev. Lett., **99**, 110602-1 (2007).
 - ¹⁵ Zs. Radi, P. B. Barna, Surf. and Coat. Techn., **100-101**, 90. (1998).
 - ¹⁶ A. Csik, G. A. Langer, D. L. Beke, Z. Erdélyi, M. Menyhárd, A. Sulyok, J. Appl. Phys., **89** 804 (2001), Z.

- Erdélyi, G. A. Langer, A. Csik, D. L. Beke, *Diff. Def. Forum* **264**, 91 (2007).
- ¹⁷ G. Quyang, C. X. Wang, G. W. Yang, *Appl. Phys. Lett.*, **86**, 171914 (2005).
 - ¹⁸ P. Delugas and V. Fiorentini, *Phys. Rev.* **B69**, 085203 (2004).
 - ¹⁹ D. K. Avasthi, W. Assmann, A. Tripathi, S. K. Srivastava, S. Ghosh, F. Grner, and M. Toulemonde, *Phys. Rev.* **B68**, 153106 (2003).
 - ²⁰ C. Melis, G. M. Lopez, and V. Fiorentini *Appl. Phys. Lett.* **85**, 4902 (2004).
 - ²¹ S. Solmi and M. Bersani, *J. Appl. Phys.* **87**, 3696 (2000).
 - ²² D. R. Sparks, R. G. Chapman, and N. S. Alvi, *Appl. Phys. Lett.* **49**, 525 (1986).
 - ²³ V.C. Venezia, R. Duffy, L. Pelaz, M.J.P. Hopstaken, G.C.J. Maas, T. Dao, Y. Tamminga and P. Graat, *Materials Science and Engineering* **B124-125**, 245 (2005).
 - ²⁴ W. F. J. Slijkerman, P. M. Zagwijn, J. F. van der Veen, G. F. A. van de Walle, and D. J. Gravesteijn, *J. Appl. Phys.* **70**, 2111 (1991).
 - ²⁵ R. Metzler, J. Klafter, *Phys. Rep.*, **339**, 1. (2000), R. Guantes, J. L. Vega, S. Miret-Artés, *Phys. Rev.*, **B64**, 245415 (2001).
 - ²⁶ R. van Gastel, E. Somfai, W. van Saarloost, J. W. M. Frenken, *Nature*, **408**, 665 (2000), D. Brockmann, T. Giesel, *Phys. Rev. Lett.*, **90**, 170601-1 (2003), R. Guantes, J. L. Vega, S. Miret-Artés, *Phys. Rev.*, **B64**, 245415 (2001).
 - ²⁷ W.D. Luedtke and U. Landman, *Phys. Rev. Lett.* **82**, 3835 (1999).
 - ²⁸ T. Michely, J. Krug, *Island, Mounds and Atoms*, Springer (2004).
 - ²⁹ P. Süle, *Surf. Sci.*, **585**, 170 (2005).
 - ³⁰ P. Süle, M. Menyhárd, K. Nordlund, *Nucl Instr. and Meth. in Phys. Res.*, **B222**, 525 (2004).
 - ³¹ P. Süle, *submitted for publication*, www.mfa.kfki.hu/~sule/papers/ptonal.pdf and [cluster.pdf](http://www.mfa.kfki.hu/~sule/papers/cluster.pdf).
 - ³² P. Ohresser, H. Bulou, S. S. Desi, C. Boeglin, B. Lazarovits, E. Gaudry, I. Chado, J. Faerber, F. Scheurer, *Phys. Rev. Lett.* **95**, 195901-1 (2005).
 - ³³ K. Nordlund, J. Keinonen, M. Ghaly, and R. S. Averback, *Nature (London)*, **398**, 49 (1999).
 - ³⁴ M. Yakes, M. Hupalo, M. A. Zaluska-Kotur, Z. W. Gortel, and M. C. Tringides, *Phys. Rev. Lett.* **98**, 135504 (2007).
 - ³⁵ H. Bulou, J-P. Bucher, *Phys. Rev. Lett.* **96**, 076102 (2006).
 - ³⁶ P. Süle, M. Menyhárd, *Phys. Rev.*, **B71**, 113413 (2005).
 - ³⁷ D. L. Beke, Z. Erdélyi, *Phys. Rev.* **B73**, 035426 (2006), Z. Erdélyi, M. Sladeczek, L.-M. Stadler, I. Zicak, G. A. Langer, M. Kis-Varga, D. L. Beke, and B. Sepiol, *Science* **306**, 1913 (2004).
 - ³⁸ M. Nastasi, J. W. Mayer, J. K. Hirvonen, *Ion-Solid Interactions: Fundamentals and Applications*, Cambridge, (1996).
 - ³⁹ R. S. Averback, T. Diaz de la Rubia, *Solid State Physics* **51**, 281. (1998)
 - ⁴⁰ A. Barna, M. Menyhárd, L. Kótis, Gy. J. Kovács, G. Radnóczy, A. Zalar, and P. Panjan *J. Appl. Phys.* **98**, 024901 (2005)., M. Menyhárd, P. Süle, *Surf. Interf. Anal.* **39**, 487 (2007), P. Süle, M. Menyhárd, *Diff. Def. Forum* **264**, 19 (2007), A. Barna, *et al.*, *Appl. Surf. Sci.* **242**, 375 (2005).
 - ⁴¹ A. L. Vázquez de Parga, J. M. Gallego, J. J. de Miguel and R. Miranda, *J. Phys.: Condens. Matter* **14**, 4187. (2002), H. F. Yan, Y. X. Shen, H. B. Guo and B. X. Liu, *J. Phys.: Condens. Matter* **19**, 026219. (2007).
 - ⁴² S. Zhao, T. C. Germann, and A. Strachan, *J. Chem. Phys.* **125**, 164707 (2006).
 - ⁴³ S. Balasubramanian, S. W. Mansour, M. R. Melloch, D. D. Nolte, *Phys. Rev.* **B63**, 033305 (2001).
 - ⁴⁴ V. V. Chaldyhehev, *et al.*, *Appl. Phys. Lett.* **79**, 1294 (2001).
 - ⁴⁵ H. Gnaser, *Low-energy Ion Irradiation of Solid Surfaces*, in *Solid-State Physics*, Springer (1999)
 - ⁴⁶ R. A. Gonzáles, F. Yubero, J. M. Sanz, *Low Energy Ion Assisted Film Growth*, Imperial College Press, London, (2003).
 - ⁴⁷ P. Süle, M. Menyhárd, K. Nordlund, *Nucl Instr. and Meth. in Phys. Res.*, **B226**, 517 (2004), **B211**, 524 (2003).
 - ⁴⁸ M. A. Karolewski, *Nucl. Instrum. Meth. in Phys. Res.* **243**, 6 (2006).
 - ⁴⁹ B. J. Thijsse, T. P. C. Klaver and E. F. C. Haddeman, *Appl. Surf. Sci.*, **231-232**, 29 (2004).
 - ⁵⁰ H. L. Meyerheim, V. Stepanyuk, A. L. Klavskyuk, E. Soyka, J. Kirschner, *Phys. Rev.* **B72**, 113403 (2005).
 - ⁵¹ TRIDYN, FZR-317, W. Möller and M. Posselt, Forschungszentrum Rossendorf, 01314 Dresden, Germany, W. Möller, W. Eckstein, J. P. Biersack, *Comput. Phys. Comm.* **51**, 355 (1988).
 - ⁵² M. Menyhárd, *Surf. Interface Anal.* **26** 1001 (1998).
 - ⁵³ K. Nordlund, *Comput. Mater. Sci.*, **3**, 448. (1995), K. Nordlund, J. Tarus, J. Keinonen, S.E. Donnelly, R.C. Birtcher, *Nucl. Instr. and Meth. in Phys. Res.* **B206** 189 (2003),
 - ⁵⁴ M. P. Allen, D. J. Tildesley, *Computer Simulation of Liquids*, (Oxford Science Publications, Oxford 1989)
 - ⁵⁵ C. Goyhenex, H. Bulou, J.-P. Deville, and G. Trolia, *Phys. Rev.* **B60**, 2781 (1999).
 - ⁵⁶ N. A. Levanov, V. S. Stepanyuk, W. Hergert, D. I. Bazhanov, P. H. Dederichs, A. Katsnelson, and C. Mas-sobrio, *Phys. Rev.* **B61**, 2230 (2000).
 - ⁵⁷ W. Eckstein, *Computer Simulation of Ion-Solid Interactions*, (Springer, Berlin 1991).
 - ⁵⁸ V. Rosato, M. Guillope, G. Mazzone, *Phil. Mag.* **A59**, 321 (1989), F. Cleri, G. Mazzone and V. Rosato, *Phys. Rev.* **B47**, 14541 (1993), F. Cleri and V. Rosato, *Phys. Rev.* **B48**, 22-33 (1993).
 - ⁵⁹ M. J. Frisch, G. W. Trucks, H. B. Schlegel, *et al.*, Gaussian, Inc., Pittsburgh PA, (2003), see also at: <http://www.gaussian.com>.
 - ⁶⁰ P. Hohenberg and Kohn, *Phys. Rev.* **136**, 864 (1964), W. Kohn and L. J. Sham, *Phys. Rev.* **140**, 1133 (1965).
 - ⁶¹ P. J. Hay, W. R. Wadt, *J. Chem. Phys.*, **82**, 6026 (1985).
 - ⁶² J. P. Perdew, K. Burke, and M. Ernzerhof, *Phys. Rev. Lett.* **77**, 3865 (1996).
 - ⁶³ C. Ambrosch-Draxl, P. Süle, H. Auer, and E. Ya. Sherman, *Phys. Rev.* **B67**, 100505 (2003), P. Süle, S. Kurth, and V. E. Van Doren, *Phys. Rev.* **B60**, 5429 (1999), P. Süle and Á. Nagy, *J. Chem. Phys.* **104**, 8524 (1996).
 - ⁶⁴ <http://www.mfa.kfki.hu/~sule/animations/ptti.htm>.
 - ⁶⁵ Y.-T. Cheng, *Mater. Sci. Rep.* **5**, 45 (1990).
 - ⁶⁶ F. Besenbacher, F. J. Bottiger, S. K. Nielsen, H. J. Whitlow, *Appl. Phys.* **A29**, 141 (1982).
 - ⁶⁷ E. Ma, T. W. Workman, W. L. Johnson, M.-A. Nicolet, *Appl. Phys. Lett.* **54**, 413 (1989).
 - ⁶⁸ G. Martin, P. Bellon, *Solid State Phys.* **50**, 189 (1997). G. Martin, *Phys. Rev.* **B30**, 1424 (1984).
 - ⁶⁹ J. W. Cahn, *Acta Metall.*, **9**, 795 (1961), J. W. Cahn, J. E. Hilliard, *ibid*, **19**, 151 (1971).